

The Bubble Challenge for High-Speed Photography

Werner Lauterborn and Thomas Kurz

Abstract Bubbles in liquids show a rich set of phenomena ranging from harmless gaseous bubbles rising in a liquid to almost empty cavitation bubbles responsible for the destruction of ship propellers. A special property of bubbles are the extremely high-speed liquid flows they enable by providing almost empty space for acceleration. Thus bubble dynamics presents a challenge for proper investigation, in particular high-speed liquid jet formation and shock wave radiation. One tool developed to study fast dynamics is high-speed photography with suitable cameras. The gradual approach to resolve bubble dynamics, in particular bubble collapse, via ever too slow cameras up to the state of the art of some hundred million frames per second is reviewed. Some ideas on the numerical extension of camera speed limits are put forward. Moreover, the first historic steps into getting three-dimensional images recorded via high-speed holography with up to some hundred thousand holograms per second are reported.

1 Historic Reflections

Already the old Greeks knew that to stop a motion one should have a short glimpse only at an object, e.g. an arrow. In the limit of shorter and shorter glimpses the object comes to a standstill, that is, no motion is to be perceived at all. This led

Electronic supplementary material The online version of this chapter (doi:[10.1007/978-3-319-61491-5_2](https://doi.org/10.1007/978-3-319-61491-5_2)) contains supplementary material, which is available to authorized users.

W. Lauterborn (✉) · T. Kurz
Drittes Physikalisches Institut, Georg-August-Universität Göttingen,
Friedrich-Hund-Platz 1, 37077 Göttingen, Germany
e-mail: Werner.Lauterborn@phys.uni-goettingen.de

T. Kurz
e-mail: Thomas.Kurz@phys.uni-goettingen.de

Zeno of Elea to argue that there can be no motion in the world, a paradoxon. Of course, there is motion in the world, but by this and other paradoxa Zeno made motion a problem to think about. Zeno could not solve the motion problem himself—in essence the problem of how to define velocity—but in the course of history mankind learned that one must look *two* times at an object to detect a motion and determine its velocity. Then, from the respective locations of the object at the two times and the time difference a velocity can be defined.

The question, however, remains what the object has done in between the two glimpses that today are realized by suitable cameras with short exposure time, the equivalent of a short glimpse for a camera. Sometimes, an object changes appreciably even when the time interval between the two exposures is very short. Then either the time interval has to be shortened or, when technical constraints do not allow this option, an interpolation has to be done—either mathematically, e.g. by linear interpolation, or according to the applicable laws of nature when known. To stay with the case of an arrow launched from a bow, instead of a mathematical linear interpolation a parabola may be fitted to the measurements as gravity is expected to act in this case. A modern example is a tennis or soccer ball that is followed by high-speed photography and subsequent curve fitting to decide, whether the ball has touched or crossed a line. In the case of a bubble in a liquid, as considered here, the Navier-Stokes equation or simpler equations derived from them would be chosen for interpolation.

It was not before the invention of photography and its cameras that whole scenes with fast moving objects could be stopped in their motion by short exposure times. Already a single high-speed photograph is able to reveal details of a process or phenomenon not to be detected by normal human perception. One prominent example is a bullet smashing a bulb. Here, the case of a bubble in a liquid is taken to exemplify the achievements of high-speed photography. Bubbles in a liquid are particularly suited for this purpose because there exists a variety with very peculiar and extremely fast dynamics that presents a challenge till today. In particular, cavitation bubbles—almost empty bubbles that appear in a liquid upon rupture by too strong tension or too high local energy deposit—may collapse so violently that shock waves are radiated, light is emitted and the hardest materials are destroyed. Material pitting was first noticed in the destruction of ship propellers and became known as cavitation erosion. There is ongoing research on this topic and bubble dynamics near surfaces in general. Some examples of bubble dynamics near a flat, solid wall can be found in this article.

Bubbles seldom come alone and thousands of them may occupy a three-dimensional volume. To stop and follow their motion high-speed holography has been invented. Some early devices constructed in connection with bubble dynamics will be discussed.

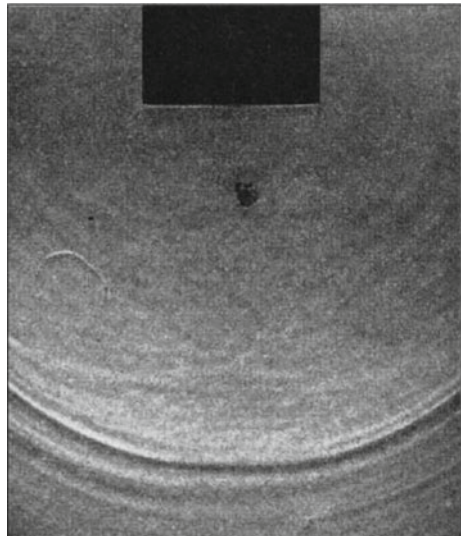
2 To Stop a Motion

To stop a motion exposure times must be chosen according to the speed of the object in question, the higher the speed the shorter the exposure time to arrive at a sharp image. Object speeds range from slow motions (0 m/s in the lower limit) to the speed of light (about 300,000 km/s in the higher limit). At very low speeds, for instance of a snail, exposure times of seconds may be appropriate. These were the exposure times possible at the beginning of photography because of the then very low sensitivity of the photographic material and the low intensity of the available light sources. At moderate speeds, for instance in athletics sports, below a millisecond (10^{-3} s) is often needed to catch specific instants of human motion. Exposure times in this range can be realized by mechanical shutters.

At high speeds, for instance of a bullet, lower exposure times in the order of microseconds (10^{-6} s) or less are necessary to stop the motion for inspection. These motions and faster ones are beyond human perception speed. Exposure times in this range and beyond are usually realized by short flashes of light as can be obtained by sparks or nowadays by short pulses of laser light.

At very high speeds, for instance in explosions or motions with the speed of sound (about 1500 m/s in water) or with supersonic speeds (shock waves), even lower exposure times of down to nanoseconds (10^{-9} s) may be needed to stop the motion. An example of how such a motion can be caught is given in Fig. 1. A bar (the black rectangle in Fig. 1) oscillating at 2.4 kHz up and down is generating a cavitation bubble cloud below it that periodically or almost periodically collapses (dark spot in the middle of the picture) with emission of shock waves from the individual bubbles. The exposure time in this case is determined by an illuminating

Fig. 1 Shock waves in water from a collapsing bubble cloud in an acoustic field of frequency 2.4 kHz. Photography with 500 ns exposure time from a light flash. See also Kuttruff 1962 [1]



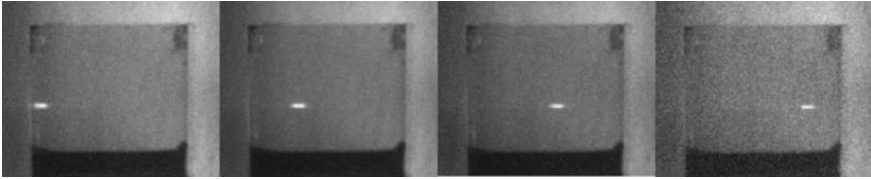


Fig. 2 A bullet of light propagating in water. The motion has been stopped with exposure times in the femtosecond range

flash of 500 ns duration from a spark source in a schlieren arrangement to make the shock waves visible (the dark and bright arcs below the collapsed bubble cloud). This way, the event has been caught and can be inspected on a larger, humanly accessible time scale. Here, the shock waves and the light emitted by the bubbles upon collapse (sonoluminescence) were of interest [1]. This topic surfaced about thirty years later because of the incredible violence and speed of the process of bubble collapse and the phenomena related with it [2].

At the ultimate speed, the speed of light, exposure times also approach their limit. Picoseconds (10^{-12} s) to femtoseconds (10^{-15} s) must be employed to stop motions near or at the speed of light. *Light in flight* is an extreme example. In Fig. 2 a bullet of light (a very short light pulse in the femtosecond range or shorter) is almost stopped in its motion through a cuvette filled with water and scattering particles by a light activated shutter. A succession of single pictures with increasing delay between repeated propagating ultrashort light pulses and an ultrashort shutter light pulse (of actually the same duration) demonstrates the propagation of light by stopping its motion by the very short *glimpses* thus provided. For details of the arrangement see Fig. 11.22 in the book by Lauterborn and Kurz [3].

This example leads us to the topic of how a motion may be followed. When a motion can be repeated identically, then a proper succession of pictures with time delay between repeated motions gives the illusion of a real motion, actually it can be considered the real motion itself. This principle is used in sampling oscilloscopes in the case of identically repeating electronic signals. However, it may be a fake motion, as the backwards rotating wheels of vehicles in movies reveal. This means that the time difference between one exposure and the next one must be short enough with respect to the real motion or properly chosen in the case of repeating motions. When this demand cannot be fulfilled as in a movie with a fixed time difference between exposures, false motion impressions may be the result.

3 To Follow a Motion

As already stated, the exposure time to get a sharp image from a fast motion must be sufficiently short. But also the time difference between one picture (frame) and the next must be sufficiently short (usually larger than the exposure time). Otherwise

the object (a light bullet, for instance) may have escaped the field of view. Or a whole scene with different objects may have altered so strongly that the different motions in the scene cannot be discerned. For slow object motions, the film material can be transported from frame to frame for the next exposure as in a normal camera or in movie cameras. This principle soon reaches its speed limit, as the film has to be moved and stopped at a faster and faster pace for faster and faster motions.

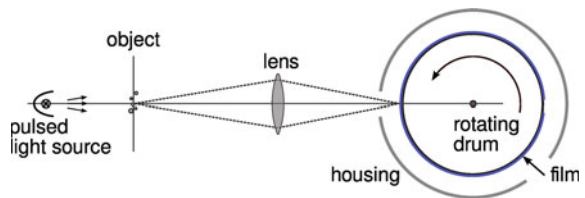
3.1 Rotating Drum Camera

Higher speeds of the film material can be reached without stopping the film for each exposure. Then the illumination of the scene must be short enough so that the additional motion of the film does not matter. This principle is realized in the rotating drum camera (Fig. 3). There, the film is placed around the outer periphery of a drum in a light-tight housing and the drum is set into rotation. A slit in the housing behind an objective lens can be opened for the time of one rotation by a mechanical shutter and a series of flashes is illuminating the object in question. The repetition rate of the flashes has to be set according to the speed of the film and the width of the slit for placing one image aside the neighbouring one. The flashes themselves have to be short enough for not to blur the image on the moving film.

An example of a relatively slow motion captured with the help of a rotating drum camera is given in Fig. 4, left four columns [4]. A drop is falling down onto a water surface, produces a splash and pushes water aside to leave about a half sphere of air below the water surface. When this half sphere closes, a water jet is shooting upwards with a drop on top. The picture series had been taken at 300 frames/s, but already at this low framing rate the succession of the events caught is beyond human perception speed. In this case, the frames have individually been taken from the film material and arranged for most compact presentation. For the latest developments in drop impact see Visser et al. [5].

An example of a faster process that could be resolved with the help of a rotating drum camera is the visualization of the gross succession of events following the focusing of a short light pulse of a ruby laser (about 30–50 ns duration) into water (Fig. 4, right two columns). The process has been slowed down by lowering the static pressure in the flask filled with water down to about half the ambient pressure. Then 6000 frames/s are sufficient to provide an overview of the motion. The intense light leads to a breakdown of the liquid and the formation of a bubble,

Fig. 3 Principle of a rotating drum camera



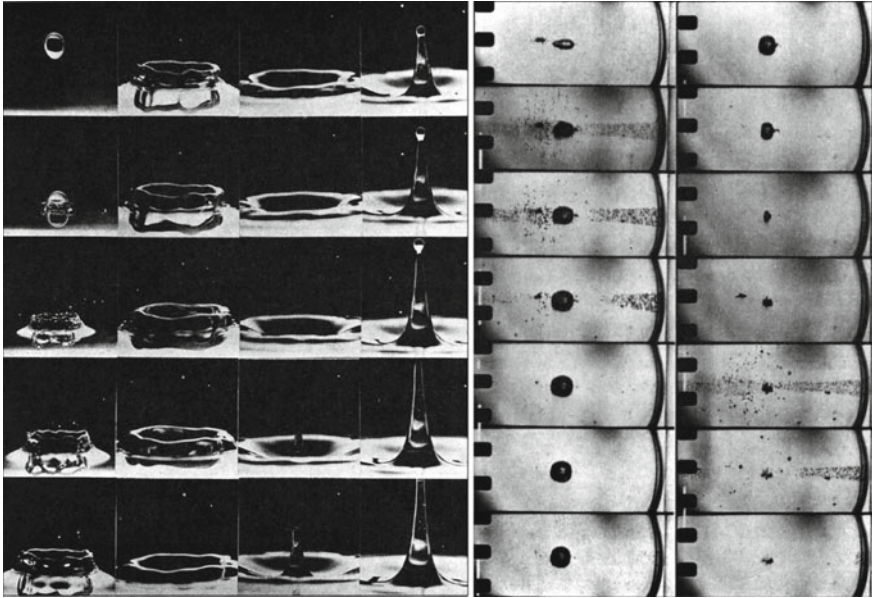


Fig. 4 *Left* Water drop impinging on a water surface. Rotating drum camera, 300 frames/s, front illumination. *Right* The successions of events when a high intensity light pulse of a ruby laser is focused into water (laser beam from the *right*). Rotating drum camera, 6000 frames/s, backlight. Time is proceeding from *top* to *bottom* and then to the next column *right*. See also Lauterborn [4]

a phenomenon called optic cavitation. The bubble expands up to a maximum size and collapses later to a smaller size. The focusing light cone becomes visible by a dense cloud of small bubbles. The bubble cloud reappears later after bubble collapse. The appearance of the bubble cloud is connected with the strong shock wave that is generated at breakdown of the liquid together with the bubble and again at bubble collapse. The shock waves themselves could not be captured optically here, because of the speediness of the shock wave propagation and therefore blurring of its motion and/or escape from the frames.

Also the rotating drum camera has its framing rate limit. The film material is moving at high speed on the circumference of a drum and is subjected to enormous centrifugal forces from its circular motion. Indeed, it happens at extreme speed that the film material ruptures and only flakes remain in the housing. Up to about 100,000 frames/s can be reached at maximum, when the slit is brought down to about 1 mm height. That means, the height of the image has to be diminished more and more to achieve higher framing rates until it becomes too small to obtain significant two-dimensional (2D) information.

However, a new principle is then emerging. When the slit is becoming very small, a 1D slice through the object is imaged in rapid succession called a streak image. Figure 5 shows an approach to a streak image with a small image height, necessary at a framing rate of 50,000 frames/s. When following the outer boundary

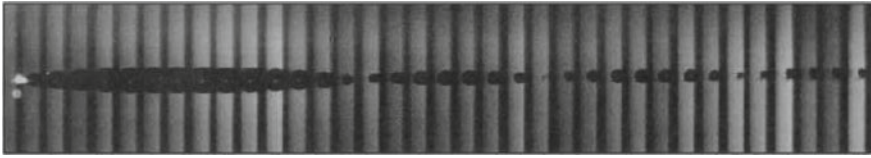
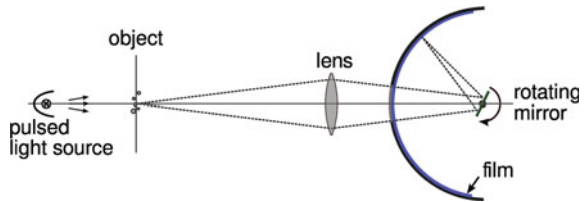


Fig. 5 Bubble formation and oscillations after a high intensity light pulse of a ruby laser is focused into water. Rotating drum camera, 50,000 frames/s

Fig. 6 Principle of a rotating mirror camera. Redrawn after Güth [7]



of the bubble, its growth with subsequent collapse, rebound (regrowth of the bubble to a second, smaller maximum) with second collapse, etc., can intuitively be followed. When the slit is very small, there is no longer a need for short pulses, as the slit together with the moving film acts as a fast shutter. This principle is used advantageously to visualize the propagation of spherical shock waves, where a 1D slice is sufficient for determining the (may be varying) speed of the shock wave. A modern example can be found, for instance, in the work of Noack and Vogel [6]. Very fast 1D motions can be measured by this type of high-speed photography. Up to 6 km/s have been found for the propagation speed of the shock wave emitted during laser-induced breakdown in water [6].

3.2 Rotating Mirror Camera

Higher framing rates than with a rotating drum camera can be obtained by a new principle, when not the film material is moved, but only a mirror rotated that projects the image of a scene onto a stationary film. The principle of a rotating mirror camera is given in Fig. 6. An objective lens images an object via a mirror onto a stationary stripe of film material that is located on a circle around the axis of rotation of the mirror. When the illumination consists of short enough flashes, one image is laid aside the previous one and a whole sequence of images can be obtained as in the case of the rotating drum camera. But now up to about one million frames per second can be reached. Moreover, also at slower framing rates, but high ones for a rotating drum camera, there is the advantage of larger individual images of a series and thus greater resolution of details.

Figure 7 gives an example of a comparably *slow* framing rate for a rotating mirror camera: 75,000 frames/s. Shown is a sequence of the motion of a

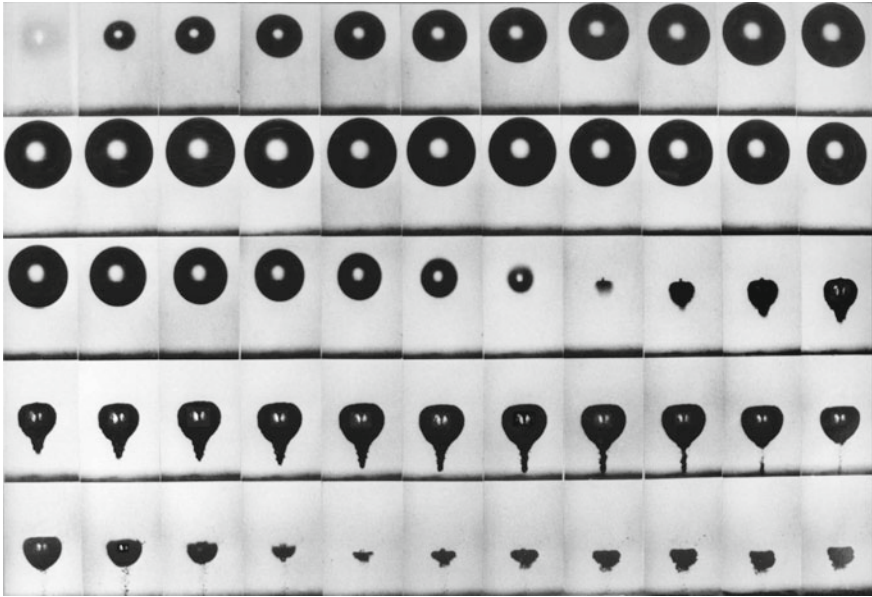


Fig. 7 Bubble dynamics near a flat, solid boundary (*lower dark line* in each frame). Rotating mirror camera, 75,000 frames/s, backlight. The maximum bubble radius is 2.0 mm and the distance of the bubble centre at maximum from the boundary is 4.9 mm. Frame size is 7.2 mm \times 4.6 mm. Time runs from *left to right* and *top to bottom*. See also Lauterborn and Bolle [8]

laser-induced bubble near a flat, solid wall as taken by Lauterborn and Bolle [8]. The bubble appears black on a bright background, because the light from the back is reflected at the bubble wall, but with a bright spot at the centre, where the light passes undeflected. Bubbles near walls are very common and encountered with ship propellers and cleaning baths, for instance. For long time, their motion could not be followed by lack of suitable high-speed cameras and thus also the process of cavitation erosion could not reasonably be investigated. With laser-induced bubbles and the progress in framing speed high resolution bubble dynamics studies became possible in the nineteen seventies [4, 8] and flourished in the next decades [9], Philipp and Lauterborn [10]. In Fig. 7 the bubble first expands as in Fig. 4 and after reaching its maximum radius collapses in a characteristic way. The collapse proceeds aspherically. One part of the liquid shoots through the bubble (to be seen as the dark line in the bright spot in the centre of the bubble) and sticks out at the opposite side, a phenomenon called jet formation. Near a flat, solid wall in a stationary liquid the jet is directed through the bubble towards the wall. This has been found—in the course of time—to be the most common type of bubble collapse, when absolutely spherical conditions cannot be guaranteed. The initiation of the jet is not really resolved in this sequence. Rather, the jet is only to be seen after its formation and best upon expanding and shrinking of the bubble in the last but one row.

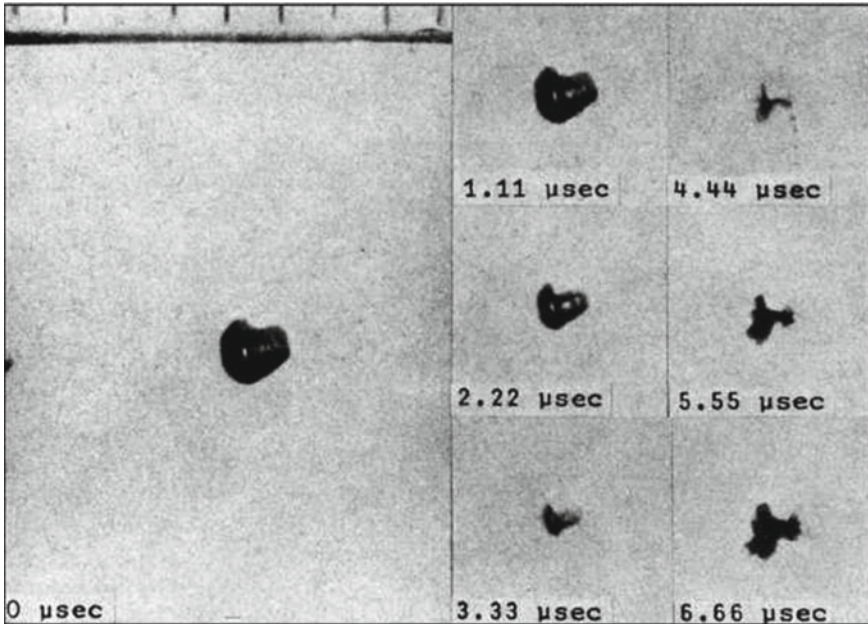


Fig. 8 Collapse of a laser-induced bubble in water. Rotating mirror camera, 900,000 frames/s. The *left* frame shows the bubble shortly before collapse together with a scale bar (1 mm distance between adjacent bars). Time runs from *top* to *bottom* and *left* to *right*. See also Lauterborn [4]

Not only jet formation, also the very collapse phase is not resolved in Fig. 7. Higher framing rates are necessary and possible with the rotating mirror camera. An example is given in Fig. 8. The sequence is taken at 900,000 frames/s. Now the collapse phase is resolved better in time and the jet formation process can be followed more closely, for instance to determine jet velocities. As discussed in the introduction, from two locations (here of the jet tip) and the two corresponding instants of time (giving the time difference, here 1.1 μ s) a velocity can be determined. That way, maximum jet velocities of 100–200 m/s were obtained, depending on the bubble size and the distance of the bubble to the wall.

A review on the application of high-speed cameras to bubble dynamics up to 1985 can be found in Lauterborn and Hentschel [11].

3.3 Image Converter Camera

From Fig. 8 it seems that the collapse of a bubble can be fairly well resolved with the help of a rotating mirror camera at its limit of about one million frames per second. However, there are collapse configurations, when this framing rate is not sufficient to follow the motion (dynamics) of a bubble. Fortunately, soon higher

framing rates became available, only limited by electronics, i.e. dispensing with mechanically movable parts and later with film material to be processed.

The development of electronic cameras with their fast electronic shutters also dispensed with the need of short illumination pulses. One of the first electronic high-speed cameras was the image converter camera. In this type of camera the light is “converted” to electrons that are multiplied in a succession of photomultiplier stages (the equivalent of the development process of a film) and delivered to a phosphor screen for converting the electrons back to light. By shifting the electrons with a high voltage onto different places on the output screen one image can be placed aside the other in fast succession. The screen is then photographed and the succession of images thus is permanently recorded. In the first version of the image converter camera the readout was made with an at that time normal camera on film. Later, with the advent of CCD cameras, also this step became fully electronic.

Shutter speeds in the range of nanoseconds can be reached, short enough for stopping the motion of shock waves. Figure 9 shows the shock waves radiated upon bubble collapse obtained by Lauterborn and Timm [12] at one million frames per second. One drawback of the image converter camera is the limited number of frames, typically eight to ten only. Therefore triggering on the collapse event by the bubble itself is necessary, see [12] and also Vogel et al. [13] and the examples therein.

The image converter camera again has its framing rate limit. It is given by the high voltage necessary to shift the electrons from one image to the next. This limit of about 20 million frames/s has been exploited by Ohl et al. [14], as a million frames per second proved not sufficient for resolving interesting details of bubble

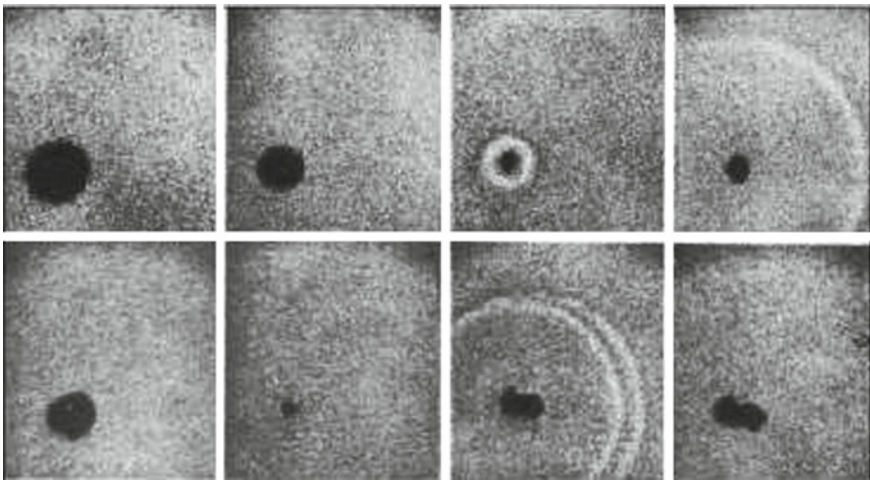


Fig. 9 Shock wave from a spherically collapsing laser-induced bubble (*upper row*) and two shock waves from an aspherically collapsing bubble with bubble splitting at collapse and merging during rebound (*lower row*). Image converter camera, one million frames per second. Width of the frames is 2.7 mm. See also Lauterborn and Timm [12]

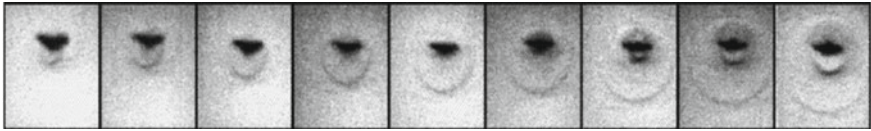


Fig. 10 Shock waves from a laser-induced bubble collapsing near a flat, *solid wall*. Image converter camera, 20.8 million frames/s. The maximum bubble radius has been 1.4 mm, the distance from the wall is 2.8 mm, the size of the frames is 1.5×1.9 mm. See also Ohl et al. [14]



Fig. 11 Shock waves from a laser-induced bubble collapsing near a flat, *solid wall* in *bottom* view. Image converter camera, one million frames per second. Frame width 4.2 mm. See also Philipp and Lauterborn [10]

collapse. Figure 10—taken at 20.8 million frames/s—reveals that the collapse phase is quite occupied with different phenomena. At least two shock waves are emitted that are separated by about 300 ns. The first one is related to the impact of the jet onto the opposite bubble wall from the interior. This event changes the topology of the bubble from simply connected (spherelike) to doubly connected (toruslike). At this instant of time the bubble still collapses further, i.e. diminishes its volume. At collapse of the torus, the second shock wave is emitted from the sudden stop of the inward motion. Only the speed-up from one million frames per second to about 20 million frames/s allowed this distinction to be made. It should be noted that it is not easy to exactly catch the collapse phenomena at this high speed in one sequence of eight frames. Therefore the sequence of Fig. 10 is a composition from different sequences with (largely) identical laser-induced bubbles.

In rare instances it happens that singular events of the collapse can be caught by chance. Figure 11 gives a sequence of three frames taken at one million frames per second with an image converter camera and CCD readout of the very moment of collapse of the torus bubble. In this case the bubble has not been photographed in side view, but from the bottom through a transparent solid boundary. The many shock waves on a ring show that the torus collapse is unstable and gives rise to many separate collapse events.

3.4 Image Splitting Camera

The—still ongoing—digital revolution that started with the hybrid image converter camera is not only able to increase the framing rate considerably, but also to speed up experimental investigations by dispensing with the time consuming processing of the film material and production of photoprints. Instead, the image sequences are available instantly and can be used to immediately direct the next measurements.

Thereby the combination of old ideas and new technology led to a new type of camera that may be called the *image splitting camera*. It is common knowledge that an image can be multiplied by partly reflecting mirrors or a scene be looked at via several mirrors and that these images can be photographed altogether *at the same time*. The new technology admits photographing each image of a mirror at slightly different times, whereby the electronic shutter and delay times between images may be as short as 5 ns. In one commercial device this is done with the help of a pyramidal image splitter to get eight (later sixteen) individual image paths. Each path is connected to a CCD camera equipped with a fast shutter down to 10 ns (later 5 ns) opening time. Together with a delay of 10 ns (later 5 ns) from one shutter (i.e. CCD camera) to the next, frame rates up to 100 (later 200) million frames per second are possible. This type of camera needs strong illumination, as only $1/(\text{number of images})$ of the light is available per image. But this demand normally is achievable by a strong xenon or LED flash. An advantage of the image splitting camera versus the image converter camera is that each image has the full frame resolution of the respective CCD camera and that each image can have its separate delay to the previous image. An example of the image quality that can be attained at a million frames per second is given in Fig. 12. It consists of two combined sequences, as only eight frames were available per measurement. Seen is a bubble at an angle of 45° from above a solid wall. The bubble is contracting with jet formation (involution from the top) passing through its collapse phase and rebounding. When looking at the collapse phase (frame 12–14), it is seen that within one microsecond the bubble considerably alters its shape, i.e. the collapse is not resolved.

A better resolution in time has already been explored with the image converter camera. However, the image splitting camera gives us the possibility to look at bubble collapse with unprecedented time and spatial resolution in the quest to reveal the secrets of bubble collapse. Figure 13 gives a composite image sequence taken at 100 million frames/s of the very collapse phase of a laser-induced bubble near a flat, solid wall in side view. The frames are labelled with the instant of time they were taken with respect to the first frame shown. The sequence covers 260 ns plus one additional frame at 300 ns. Now the jet impact phase is better time resolved and reveals much of its complex nature. As can be seen from frame 12 of Fig. 12, shortly before the jet hits the lower bubble wall, the bubble attains the shape of a (tiny) bowl. This intermediate shape lasts for a small fraction of a microsecond only. The soon following jet impingement itself proves to be an extended process in time as well as in space. Instead of touching the lower bubble

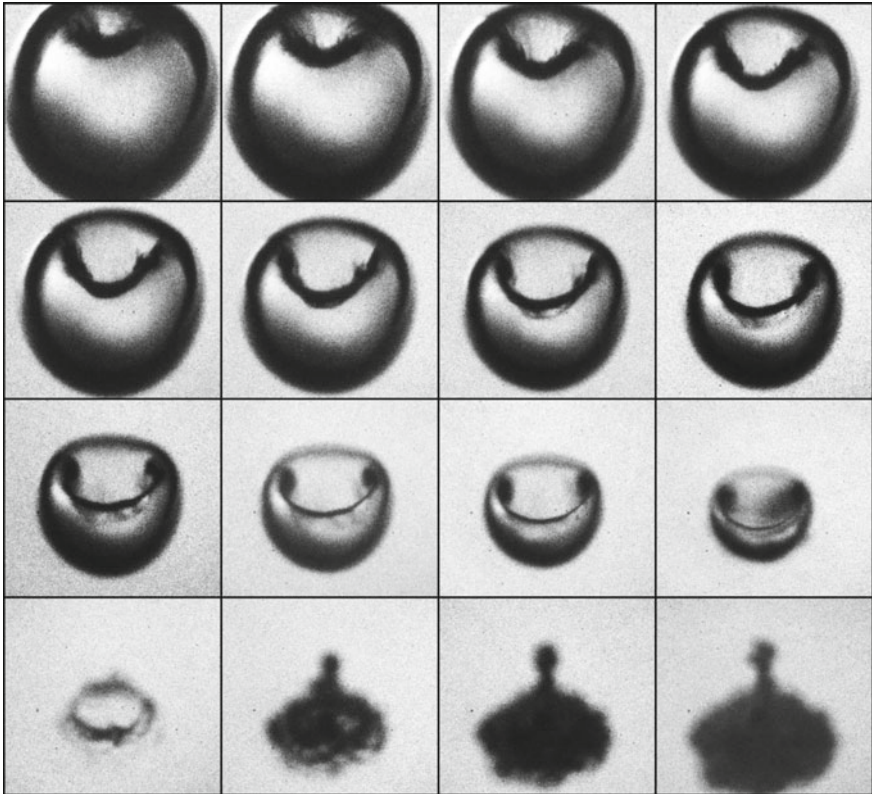


Fig. 12 Jet and counterjet formation from a laser-induced bubble collapsing near a flat, solid wall seen at an angle of 45° from above the wall. Image splitting camera, one million frames per second. Frame size 1.2 × 1.1 mm. See also Lindau and Lauterborn [15]

wall at a point, the jet hits it on a ring. This can be concluded from the two shock wave rings observed to the left and the right of the bubble in Fig. 13. The rings belong to a torus shock wave generated at the impingement ring. This is a highly sensitive situation, as only in a perfectly axially symmetric geometry a simultaneous touching of the jet at a ring will occur. The subsequent dynamics seems predetermined. The ring closing has punched out a separate bubble besides forming the torus bubble. Both bubbles will be compressed further by the fluid flow and therefore more shock waves can be expected. Moreover, a proliferation of shock waves by further liquid impacts can be taken for granted from the instability of the torus bubble (see Fig. 11).

The situation, however, is not that clear, as the torus shock wave interacts with itself and the bubble. It is not known, what effects the torus shock wave will produce inside the jet itself (not observable here), upon self-penetration along the torus axis and by diffraction around the torus bubble. At about 140 ns the torus shock wave impacts with itself on the bubble axis below the bubble at the side to

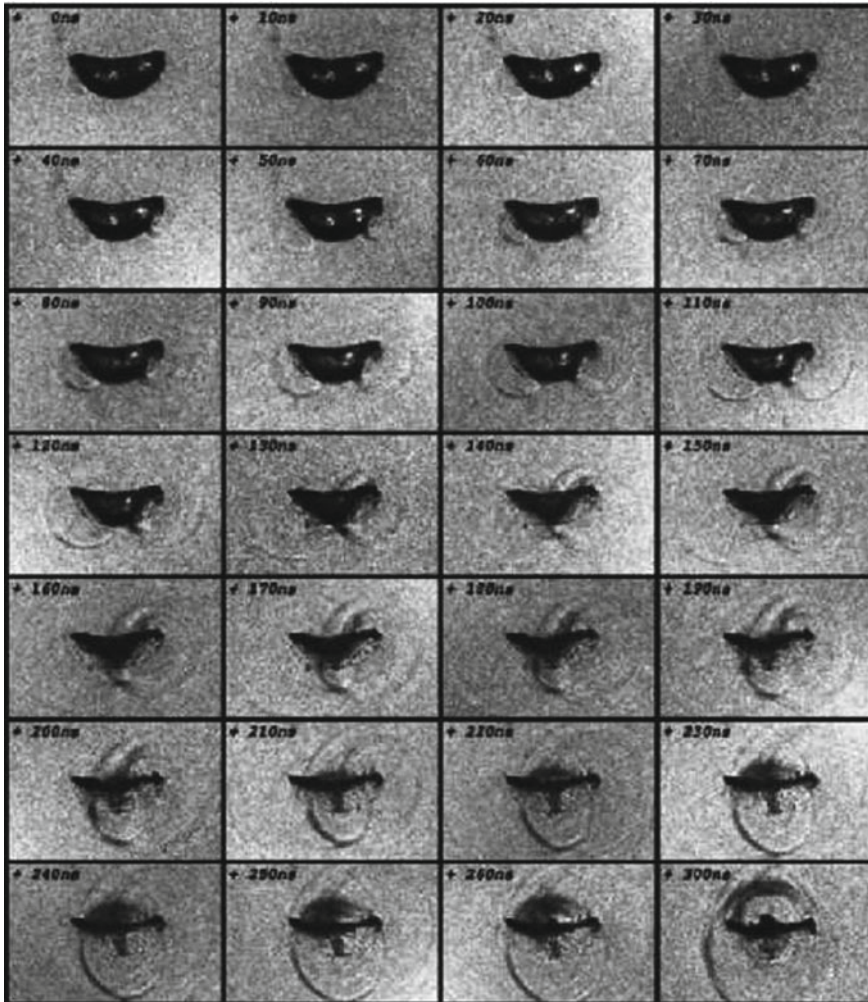


Fig. 13 Bubble dynamics and shock wave emission during bubble collapse near a flat, *solid wall* located below the bubble. Image splitting camera, 100 million frames/s. Side view and shadowgraph. Bubble radius at maximum expansion is 1.5 mm, distance of the bubble centre to the wall is 3.9 mm. Frame size is 1.3×0.8 mm. See also Lindau and Lauterborn [15]

the solid wall. It seems to be the origin of a further shock wave, presumably either from compression of the punched bubble or impact of the inflowing liquid from the main bubble collapse with the liquid of the jet. The jet is surrounded with gas and vapour from the bubble and this may be the reason for the dark granular stem to be seen from frame 170 ns onwards. It may be the remnants of the gaseous/vapourous hull of the jet after inflow of liquid from the outside towards the axis. At frame 260 ns a *nose* appears above the now flat bubble. It is of unknown origin and obviously connected with the emission of a further shock wave to be seen

expanding above the bubble. It may be connected with the *splash* observed by Tong et al. [16], a tiny ring water wave running up the inner bubble wall and impinging onto itself similar to the torus shock wave. Alternatively, it may be considered as if the inflow of liquid towards the axis is squeezing the gas hull of the main jet upwards to form the nose.

All these phenomena happen within a few hundred nanoseconds. Thereafter, on a much slower time scale, the main jet towards the solid wall forms, when the bubble is rebounding owing to the compressed gas/vapour that acts as a spring.

The main drawback of the image splitting camera is the limited number of frames of eight to sixteen that it shares with the image converter camera. Triggering on a mechanical event down to the nanosecond range for an image is exceedingly difficult. The underlying jitter from tiny deviations then may prevent to catch a fast event. New camera types are evolving that may finally reach the framing rates needed here. An order or better two orders of magnitude larger number of frames without sacrificing resolution by diminishing image height would be welcome for the time being. An unlimited stream of ultra high-speed images with post-event trigger capabilities, of course, would present the final solution for many problems.

3.5 *Numerical Extension of High-Speed Photography*

With laser-induced bubbles and high-speed photography the first calculations of jet formation of a bubble near a wall reported by Plesset and Chapman [17] could be compared with experiments by Lauterborn and Bolle [8]. The first calculations, however, could only be done up to the moment, when the jet touches the opposite bubble wall. The experiments naturally extend further in time and thus can follow the jet also further in space beyond touching the opposite bubble wall (see Figs. 7 and 8).

To jump from history to the present: it is only nowadays that numerical codes are able to proceed beyond the impact of the jet onto the opposite bubble wall (for the latest examples see Han et al. [18] and Koch et al. [19]). A comparison with the possibilities of today is given in Fig. 14 for the case of a bubble collapsing in front of a flat, solid wall with touching it upon first rebound. The right and lower part of each image shows the experimentally obtained outline of the bubble (one half) taken with a modern high-speed video camera, the left, lightly coloured rectangle the numerically obtained one by solving the Navier-Stokes equation. The lower boundary of the rectangle in each image represents the surface of the solid wall, the darker grey areas below come from the reflection of the bubble in the polished surface. To follow the jet into and in the interior of the bubble is difficult, as the outer bubble wall deflects the light and gives the view free only in the middle of the bubble, where the light passes undeflected. This is different in the numerical calculations, where a cut through the bubble can easily be done and presented as shown here. Then the jet and the formation of a torus are directly visible (each image is to be rotated along the vertical axis of symmetry, here also given by the

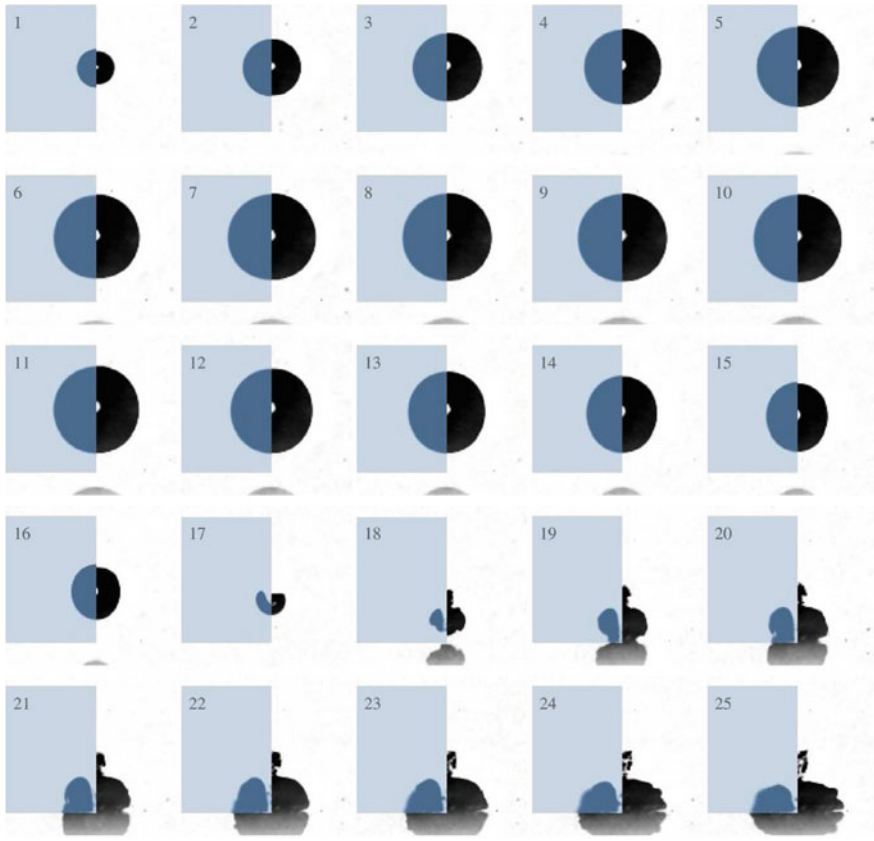


Fig. 14 Comparison of experimentally determined bubble shapes (*right and lower part of each image*) upon collapse of a laser-induced bubble in water near a flat, solid wall with numerically calculated shapes (*left in each image*). Modern high-speed video camera, 180,000 frames/s; Navier-Stokes equation solved with OpenFOAM. The maximum bubble radius is $450\ \mu\text{m}$, the distance to the boundary amounts to $642\ \mu\text{m}$. See also Koch et al. [19]

vertical numerical–experimental boundary in each composite image). The so-called *counterjet* sticking out above the experimental bubble probably is due to secondary cavitation that is not included in the bubble model. The reflection of the bubble in the boundary (best seen from frame 18 onwards) very nicely fits with the extension of the bubble in the numerical calculation. Thus, the obvious agreement over the complete sequence gives confidence into the numerical model. Then, as already put forward in the introduction, the physical model can be used to interpolate between adjacent images to get an even better time resolution than obtainable with the highest-speed cameras. Calculations of the bubble collapse with a time resolution below $0.1\ \text{ns}$ have already been done, corresponding to more than 10,000 million frames/s (M. Koch, private communication 2016). This digital extension allows an even deeper look into what we cannot see.

4 The 3D Challenge

A conventional image is a two-dimensional projection of a three-dimensional scene. As such it contains only part of the reality. The first approach to 3D consisted in simultaneously taking two projections at an angle between them, called stereoscopy. A depth perception is resulting from the parallax between the two projections. Therefore it might be applicable to measure 3D bubble distributions. This approach has been reported by Appel et al. [20]. Figure 15 gives an arrangement for studying bubble dynamics in an ultrasonic field of 22.8 kHz (acoustic cavitation). Three cameras are looking at different angles onto a bubble distribution. The three cameras, called HiSIS1 and HiSIS2 and Pulnix, are synchronized to take images at the same instants of time. Typically they are operated at 2250 frames per second by us. Figure 16 shows a result of the achievement with this arrangement. A 3D bubble distribution taken from many frames is plotted with three orthogonal planes of projection for better perceiving the 3D structure. It is seen that by no means the bubble distribution is homogeneous. Instead, the bubbles are arranged in a characteristic way with many branches (called streamers in the community). This is very unfortunate for ultrasonic cleaning, as cleaning is mediated by bubbles: no bubbles, no cleaning. Moreover, velocities of the bubbles can be deduced from the frames and velocity distributions be given [20].

Stereoscopy is like looking with two eyes, but without being able to turn the head or approaching the scene. Also the cameras have a limited depth of field and can view only a small volume at high resolution. Therefore other solutions were sought for and found in holography to be discussed next.

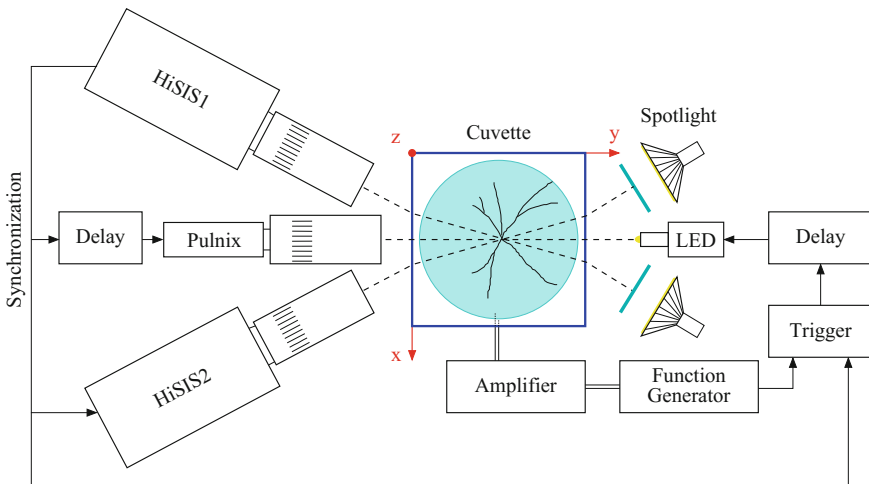


Fig. 15 Arrangement for high-speed stereoscopy of bubble distribution and bubble motion. Courtesy of R. Mettin

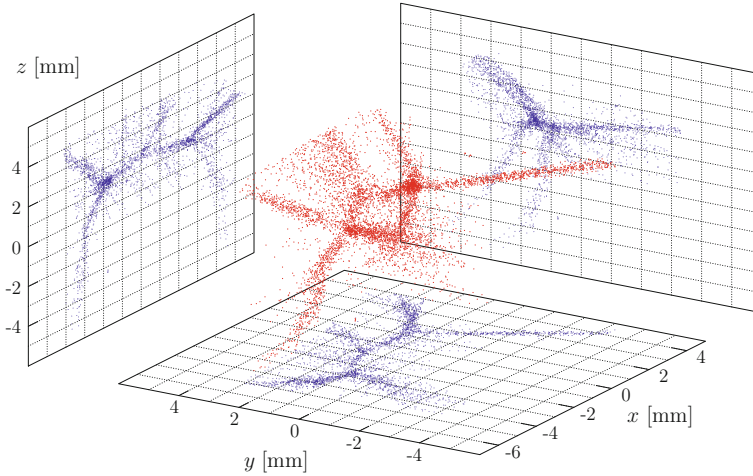


Fig. 16 Bubble distribution obtained by high-speed stereoscopy. High-speed CCD cameras, 2250 frames/s. Bubbles driven acoustically at 22.8 kHz. Courtesy of J. Appel. The corresponding videos are available online

4.1 Holographic Cameras

When a scene can be illuminated with coherent light, one can do much better in principle with a holographic camera. In holography a hologram stores the scene in an interference pattern between the light from the scene and a reference beam. Upon reconstruction from a hologram by illuminating it with the reference beam, the reconstructed 3D image can be photographed at different angles and from different distances at different magnifications. A hologram thus preserves a three-dimensional image, albeit with the restriction of looking through the hologram like through a window. With the help of the conjugate reference beam (backwards propagating reference beam passing the hologram) the 3D image can be projected into real space. Then planes through the 3D image can be intercepted and stored on film or any other photosensitive surface without any lenses or other imaging system.

Figure 17, left column, gives four planes of a reconstructed 3D image from a hologram taken on a high resolution photographic plate with a single exposure from a He-Ne laser at a wavelength of 632.8 nm [21]. The 3D scene holographed contained many bubbles on wires in water. It is seen that a very good quality of photographs can be obtained from the real image projected into space. The diameter of the wires is 40 μm only and the smallest bubbles are about 100 μm in size. Thus holography may be used for bubble studies.

With short enough coherent pulses also high-speed motions can be stopped as in conventional photography, but now in three dimensions. Any short, sufficiently coherent pulse from any laser can be used for a holographic camera. Therefore quite

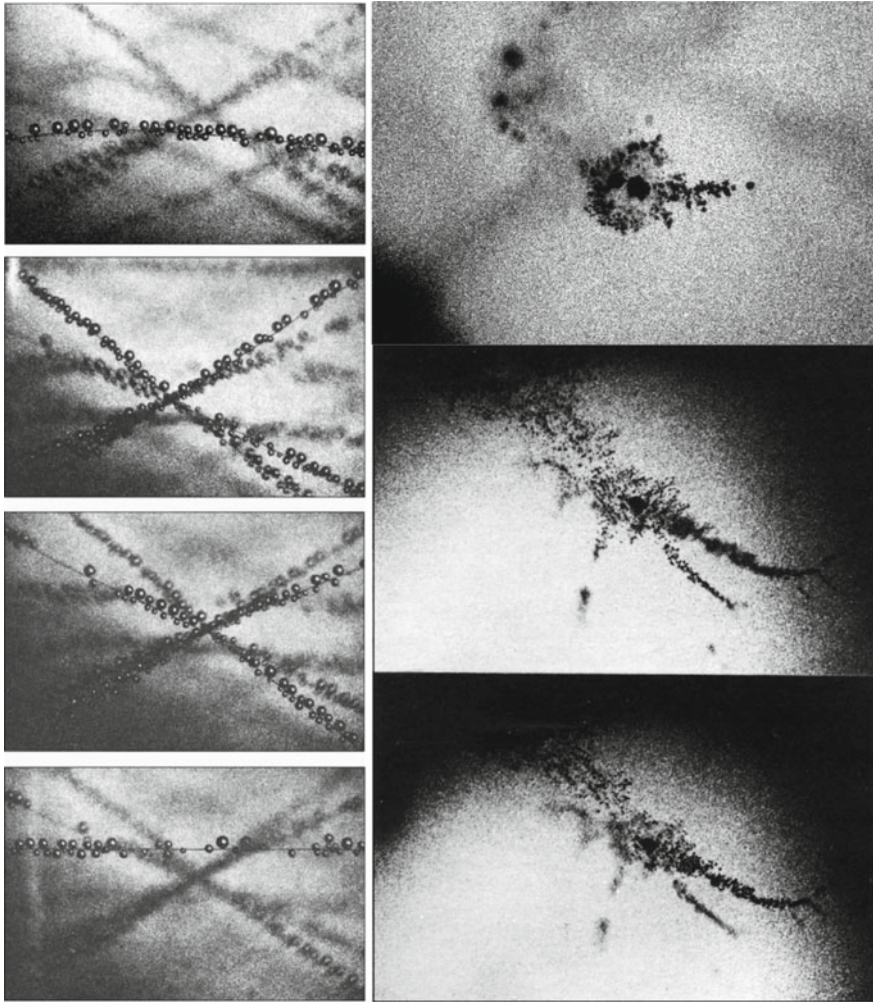


Fig. 17 *Left column* bubbles on wires in water. He–Ne laser holographic camera. Four planes covering 1.5 cm in depth from the reconstructed real image of a hologram. Diameter of a wire is 40 μm . See also Lauterborn et al. [21]. *Right column* cavitation bubble distribution in water inside a cylindrical acoustic transducer driven at 19 kHz. Photographic images from the reconstructed 3D real image of a hologram. Three different planes in depth and from different locations in the 3D image. The two lower images are about 5 mm apart. Ruby laser high-speed holographic camera. Exposure time is about 20 ns. Hologram taken in collaboration with K. Hinsch and F. Bader in 1972

different types exist depending on the wavelength. The first laser used was the ruby laser at a wavelength of 694.3 nm. By Q-switching a short coherent pulse (or also a series of pulses) can be obtained. An example is given in Fig. 17, right column. A single pulse from a ruby laser was used to holograph the cavitation bubble

distribution in water inside a cylindrical piezoelectric acoustic transducer driven at 19 kHz. The high acoustic intensity applied ruptures the water, called acoustic cavitation, and gives rise to the characteristic distribution of bubbles with many branches, the streamers, that are occupied with bubbles. They extend in three dimensions and are not easily photographed in their entirety in high resolution. Three planes from the reconstructed 3D real image are shown at different depth. Two streamers are in focus in their respective planes about 5 mm apart (lower two images). A special, but quite common bubble distribution is given in the upper 2D image from the same hologram: a comet like bubble aggregation with two larger bubbles, a halo of smaller bubbles and a tail, also made up of small bubbles. One large bubble in an acoustic cavitation bubble cloud is often accompanied by a school of small bubbles following the larger one. Presumably the small bubbles are offsprings from the larger ones in the bubble distribution, produced upon non-spherical collapse of a larger bubble.

4.2 *High-Speed Holography*

Also high-speed holographic movie cameras have been developed. Actually, they are catching a small part of the 4D world: 3D in space and 1D in time. Bubble physics has a demand for 3D images in time. In particular in acoustic cavitation—as used in cleaning baths—thousands of bubbles (that do the cleaning) are distributed in a volume of liquid. The dynamics of these bubbles is of interest.

A straightforward idea for high-speed holography is to use a rotating plate or rotating drum camera, to take a series of short coherent pulses for illumination and to add a reference beam to each of the illumination pulses. As the interference fringes may move fast and should not be blurred for good reconstructions, short enough pulses must be employed. Several different laser systems are able to deliver long series of short pulses for this purpose, e.g. the Q-switched ruby laser [22, 23], the copper vapour laser pumped dye laser [24] or the cavity dumped argon ion laser [25]. About 50,000 holograms/s of good quality can be obtained similarly to high-speed photography. Higher hologram rates have been obtained, when diminishing the hologram size (as with picture size in conventional high-speed cameras) and introducing additional deflection methods.

For short, fast hologram series (about ten holograms) the image splitting principle can be used in the form of partially reflecting mirrors. The time delay between holograms is realized by the spatial path for the image from mirror to mirror and a respective reference light delay, when the coherence length is not large enough. As a long time delay for light requires a long path in space (owing to the high speed of light) only short time delays are realizable. This corresponds to extremely high hologram framing rates. Novaro [26] could take ten holograms at 500 million holograms/s with his image splitting high-speed holographic camera. However, only near light speed dynamics can be studied with this holographic camera.

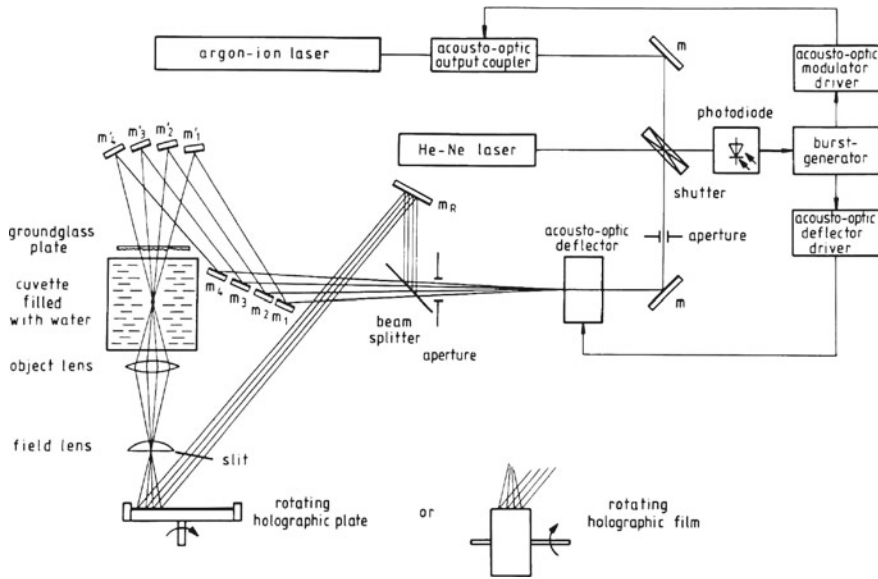


Fig. 18 Argon ion laser high-speed holographic camera with either a rotating plate or a rotating drum and additional acousto-optic beam deflection for spatial hologram separation. Limit about 300,000 holograms/s. See also Hentschel and Lauterborn [27]

Figure 18 gives a holographic arrangement for off-axis high-speed holography with an argon ion laser at a wavelength of 514 nm. It makes use of a rotating holographic plate or a rotating drum and fourfold hologram framing rate extension with a beam deflection unit as constructed by Hentschel and Lauterborn [27]. With this device up to about 300,000 holograms/s are possible [28]. An example of a holographic sequence taken at 200,000 holograms/s is given in Fig. 19. The laser-induced breakdown from focusing a Q-switched pulse of a ruby laser into water and the subsequent events are holographed. Reconstructed images from consecutive holograms are shown and numbered. The image from hologram 4 shows the shock waves radiated upon breakdown and the subsequent reconstructed images (with shifted views in columns one and four) show the growing bubble cluster and further tiny bubbles in the path of the laser beam and around the growing bubble cluster.

Image quality suffers from small hologram sizes, more than the photographic counterpart. Firstly, there is speckle in the image from the coherent light. Speckles appear at the limit of resolution, give the image a granular appearance and disturb the perception. Secondly, the hologram contains depth information and a single plane in the reconstructed 3D image therefore cannot contain the full resolution as the same plane would have in direct photography. Thus a hologram generally suffers from a resolution loss for 2D information per same area compared to conventional photography.

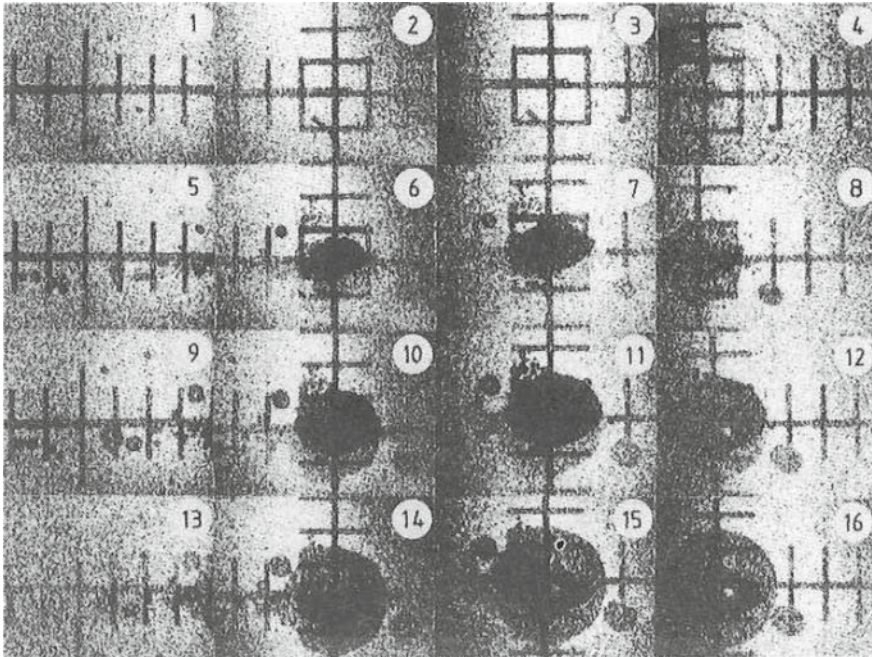


Fig. 19 Dynamics of a laser-induced bubble cloud in water. Argon ion laser high-speed rotating drum holographic camera, 200,000 holograms/s. Time runs from *left to right* and from *top to bottom*. The numbers show consecutive hologram numbers, i.e. adjacent reconstructed images are 5 μ s apart. The two *middle columns* show the growing bubble cluster, the images in the first and last column are shifted in space to the *left* and to the *right* of the main bubble cluster. Millimetre scale placed behind the bubbles. See also Hentschel and Lauterborn [28]

A similar arrangement as given in Fig. 18 has been used to holograph bubbles inside a piezoelectric cylindrical transducer (76 mm in length and diameter, wall thickness 5 mm) driven at 23.1 kHz. Inside the transducer a cloud of cavitation bubbles is generated with thousands of individual bubbles oscillating and moving around in the three-dimensional volume. The interesting fact is that with increasing driving pressure amplitude the sound emitted from the bubbles undergoes a period-doubling sequence to chaos [29]. The question was, whether the complete bubble cloud does the same. This is indeed the case as could be proven by Lauterborn and Koch [30] with the help of high-speed holocinematography (for an example of a chaotically oscillating bubble cloud taken holographically see Lauterborn and Holzfuß [31]). Holograms were taken at a rate of 69,300 holograms/s (three holograms per period of the sound field), and 3D images were reconstructed for inspection. Figure 20 shows one plane of the reconstructed images per period of the driving at the same phase of the sound field. The images are full of speckles from the coherent light, but the bubbles stand out by their clustering. When going from one image in a row to the next one, it is seen that the

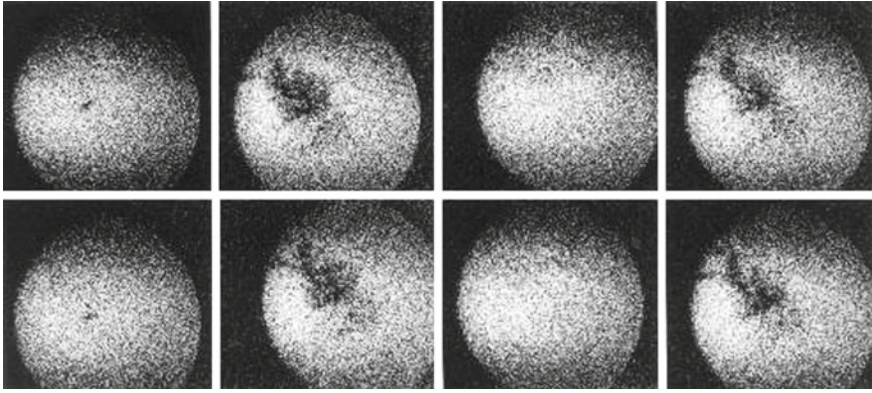


Fig. 20 Reconstructed images from a high-speed holographic sequence taken at 69,300 holograms/s of a bubble cloud driven acoustically at 23.1 kHz. Argon ion laser high-speed holographic camera. Every third image selected at a fixed phase to give one image per period of the driving. The sequence is running from *left to right* and from *top to bottom*. The bubble cloud has period doubled to at least period four. See also Lauterborn et al. [34]

bubble cloud needs at least four periods of the sound field to repeat. By careful inspection and comparison with the simultaneously taken sound emitted it is found that it needs even eight periods of the sound field for the bubble cloud to repeat.

A review on the application of high-speed holographic cameras to bubble dynamics up to 1986 can be found in Lauterborn and Hentschel [32], later in the overview by Lauterborn and Hentschel [33] and the reviews by Lauterborn et al. [34] and Lauterborn and Kurz [35].

4.3 Digital Holography

The advent of the digital computer, digital printers and digital cameras has made possible a complete digitization of the holographic process, from calculation of a hologram and plotting it, direct digital recording of a light produced hologram (the interference fringes) to numerical reconstruction from a digitally recorded hologram or from a digitized hologram on film. Subsequent digital object recognition is necessary in all cases to make (scientific) use of it.

A hologram can be computed by calculating the interference pattern from a given scene, realized by plotting it on a digital printer and reconstructed either digitally again (then no plot needed) or by illuminating it with coherent light. The last option will be a direct proof of correct calculation.

An example of a calculated binary hologram (interference fringes in black and white) is given in Fig. 21. Twenty eight points in space are coded in it, arranged in four letters, each in a different plane in depth. This can be tested by a real reconstruction with coherent light waves. To this end, the holographic pattern has to be

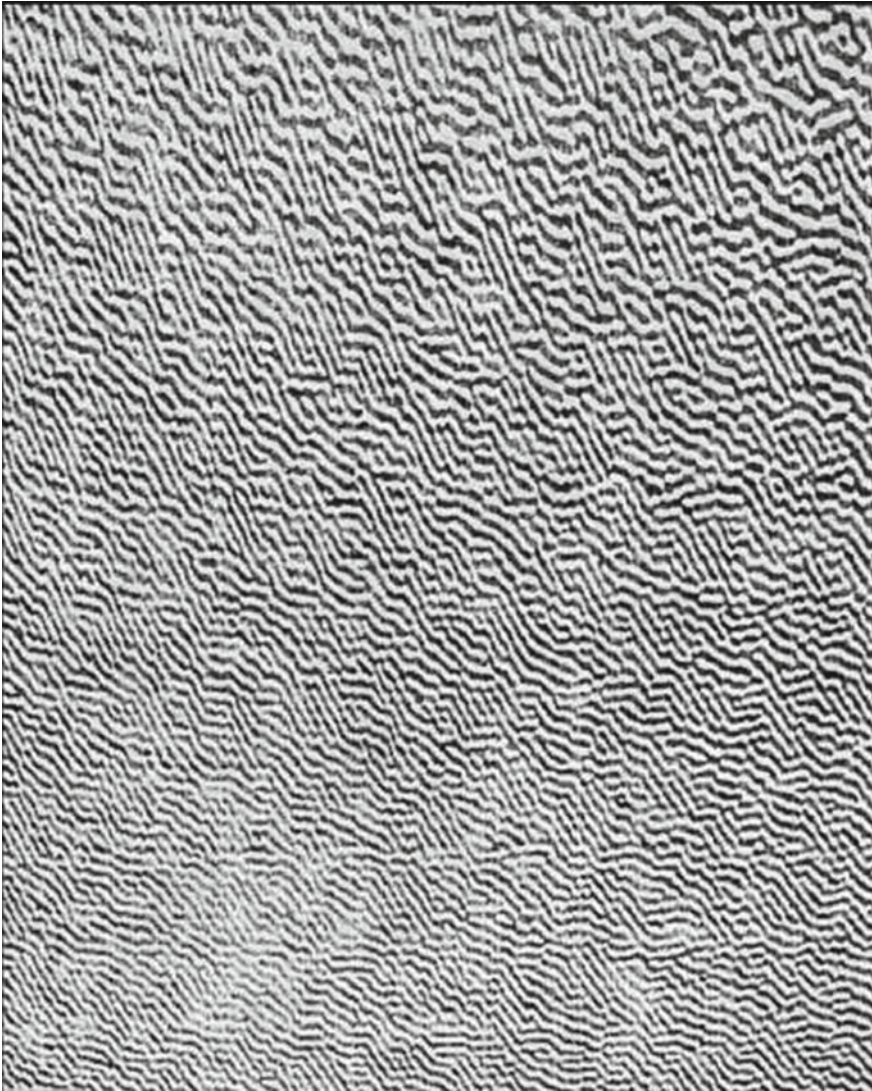


Fig. 21 Part of a computed and printed off-axis hologram in *black* and *white* (a binary hologram). It contains the word HOLO with the four letters in different planes in depth. See also Lauterborn [36]

reduced for stronger diffraction at a wavelength of visible light. In the present case, the hologram of Fig. 21 has been reconstructed from a reduction to about 5 mm edge length and illuminated with the continuous beam of a He–Ne laser (wavelength = 632.8 nm) to get the 3D image. Four photographs from the reconstructed letters are shown in Fig. 22. The 3D property of the image is clearly demonstrated.

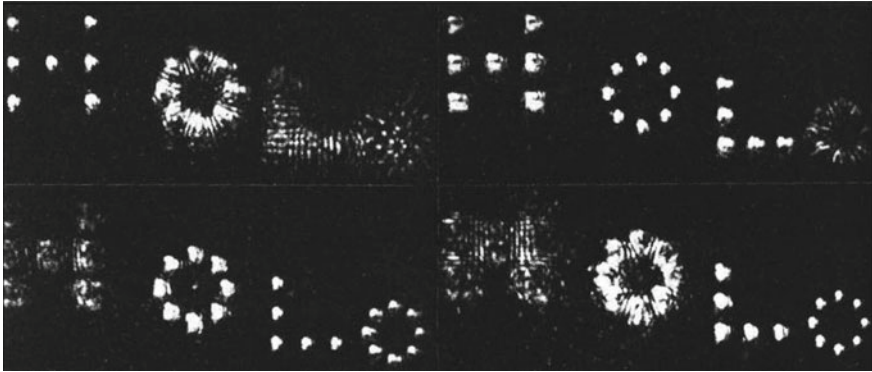
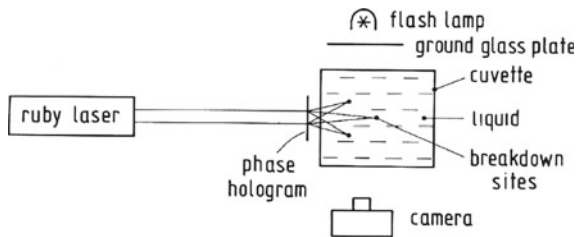


Fig. 22 Reconstructed 3D image HOLO from the binary hologram in Fig. 21 in four different views. The four different letters are located in different depths. See also Lauterborn [36]

Fig. 23 Arrangement for multiple laser-induced breakdown sites in a liquid with phase holograms. See also Lauterborn [37]



This type of digital holograms has been studied for use as lenses with multiple focal points. Then many-bubble systems can be produced in a liquid, when high intensity laser pulses are used for reconstruction. First attempts are described by Lauterborn [37] and Hentschel and Lauterborn [38]. The principle of focusing through a holographic lens is given in Fig. 23. It is a very simple arrangement, once the phase hologram is fabricated so that it can withstand the high intensities. With a similar arrangement, but with a Fourier transform hologram and an additional focusing lens, five-bubble systems have been generated in high-viscosity silicone oil (Fig. 24). Then the bubbles stick for some time to the same place and can even be seen with the naked eye.

Nowadays, digital holograms can be formed with a digital spatial light modulator (SLM) and, when properly illuminated, can be used for bubble production. Examples are given by Lim et al. [39].

The interference pattern of a hologram from a real scene can also be recorded digitally instead of on film. A proof of principle together with numerical reconstruction has been given by Schnars and Jüptner [40]. They used a CCD camera with 1024×1024 pixels with a pixel area of $6.8 \mu\text{m} \times 6.8 \mu\text{m}$. The small hologram size of about $7 \text{mm} \times 7 \text{mm}$ leads to an image with pronounced speckles. And the coarseness of the pixels with respect to the grain size of film material only allows for holographing quite far away objects at small off-axis angles.

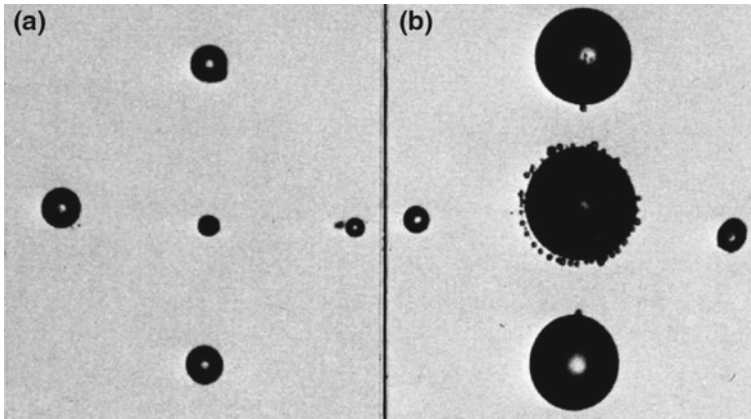


Fig. 24 Two five-bubble systems in silicone oil. Q-switched ruby laser pulse focused through a binary phase Fourier transform hologram. See also Hentschel and Lauterborn [38]

By magnifying the hologram to obtain coarser interference fringes and by using a larger number of pixels (2048×2048) Sheng et al. [41] considerably improved digital hologram recording. Modern digital cameras with their fourty and more million pixels should improve the resolution further.

The numerical reconstruction of the 3D image from a digital (or other) hologram needs further processing as to detect objects or structures in a 3D volume [42]. Also this detection process has been advanced over the years [43]. The progress over time in digital holography is documented by Schnars and Jüptner [44] and Katz and Sheng [45].

5 Summary and Conclusion

The use of different types of now historic high-speed cameras with increasing framing rates is reviewed in their application to resolve the violent motion of bubbles in liquids. Collapsing bubbles belong to the fastest mechanical objects. It was not before 100 million frames/s became available that the sequence of events during bubble collapse could approximately be resolved. High-speed holography was developed up to several hundred thousand holograms per second for observing the dynamics of spatially separated objects (bubbles in liquid) at the same instants of time. The digital revolution has brought more comfortable high-speed cameras than the historic ones and will serve for a proliferation of high-speed studies. However, the resolution of film material is still unsurmounted by a factor of ten, at least in high-speed applications.

When the time resolution cannot be increased further experimentally, a numerical extension may be possible by sophisticated interpolation. A prerequisite is that the physical laws underlying the dynamical process are known. This interpolation is presently done routinely with following tennis and soccer balls for more precise determination of impact on or aside a line. It is under way with bubble collapse impacts by using Navier-Stokes-equation interpolation and elsewhere with other physical equations. Movies from bubble collapse with the equivalent of 10,000 million frames/s are already done. Then we can see even more what we cannot see directly.

References

1. H. Kuttruff, Über den Zusammenhang zwischen der Sonolumineszenz und der Schwingungskavitation in Flüssigkeiten (On the connection between sonoluminescence and acoustic cavitation). *Acustica* **12**, 230–254 (1962)
2. D.F. Gaitan, L.A. Crum, C.C. Church, R.A. Roy, Sonoluminescence and bubble dynamics for a single, stable cavitation bubble. *J. Acoust. Soc. Am.* **91**, 3166–3183 (1992)
3. W. Lauterborn, T. Kurz, *Coherent Optics*, 2nd edn. (Springer, Berlin, 2003), pp. 234–236
4. W. Lauterborn, Kavitation durch Laserlicht (Laser-induced cavitation). *Acustica* **31**, 51–78 (1974)
5. C.W. Visser, P.E. Frommhold, S. Wildeman, R. Mettin, D. Lohse, C. Sun, Dynamics of high-speed micro-drop impact: Numerical simulations and experiments at frame-to-frame times below 100 ns. *Soft Matter* **11**, 1708–1722 (2015)
6. J. Noack, A. Vogel, Single-shot spatially resolved characterization of laser-induced shock waves in water. *Appl. Opt.* **37**, 4092–4099 (1998)
7. W. Güth, Kinematographische Aufnahmen von Wasserdampfblasen (Cinematographic recording of water vapour bubbles). *Acustica* **4**, 445–455 (1954)
8. W. Lauterborn, H. Bolle, Experimental investigations of cavitation-bubble collapse in the neighbourhood of a solid boundary. *J. Fluid Mech.* **72**, 391–399 (1975)
9. Y. Tomita, A. Shima, Mechanisms of impulsive pressure generation and damage pit formation by bubble collapse. *J. Fluid Mech.* **169**, 535–564 (1986)
10. A. Philipp, W. Lauterborn, Cavitation erosion by single laser-produced bubbles. *J. Fluid Mech.* **361**, 75–116 (1998)
11. W. Lauterborn, W. Hentschel, Cavitation bubble dynamics studied by high-speed photography and holography: Part one. *Ultrasonics* **23**, 260–268 (1985)
12. W. Lauterborn, R. Timm, Bubble collapse studies at a million frames per second, in *Cavitation and Inhomogeneities in Underwater Acoustics*, ed. by W. Lauterborn (Springer, Berlin, 1980), pp. 42–46
13. A. Vogel, W. Lauterborn, R. Timm, Optical and acoustic investigations of the dynamics of laser-produced cavitation bubbles near a solid boundary. *J. Fluid Mech.* **206**, 299–338 (1989)
14. C.-D. Ohl, A. Philipp, W. Lauterborn, Cavitation bubble collapse studied at 20 million frames/s. *Ann. Physik.* **4**, 26–34 (1995)
15. O. Lindau, W. Lauterborn, Cinematographic observation of the collapse and rebound of a laser-produced cavitation bubble near a wall. *J. Fluid Mech.* **479**, 327–348 (2003)
16. R.P. Tong, W.P. Schiffrs, S.J. Shaw, J.R. Blake, D.C. Emmony, The role of ‘splashing’ in the collapse of a laser-generated cavity near a rigid boundary. *J. Fluid Mech.* **380**, 339–361 (1999)
17. M.S. Plesset, R.B. Chapman, Collapse of an initially spherical vapour cavity in the neighbourhood of a solid boundary. *J. Fluid Mech.* **47**, 283–290 (1971)

18. B. Han, K. Köhler, K. Jungnickel, R. Mettin, W. Lauterborn, A. Vogel, Dynamics of laser-induced bubble pairs. *J. Fluid Mech.* **771**, 706–742 (2015)
19. M. Koch, C. Lechner, F. Reuter, K. Köhler, R. Mettin, W. Lauterborn, Numerical modeling of laser generated cavitation bubbles with the finite volume and volume of fluid method, using OpenFOAM. *Comp. Fluids* **126**, 71–90 (2016)
20. J. Appel, P. Koch, R. Mettin, D. Krefting, W. Lauterborn, Stereoscopic high-speed recording of bubble filaments. *Ultrason. Sonochem.* **11**, 39–42 (2004)
21. W. Lauterborn, K. Hinsch, F. Bader, Holography of bubbles in water as a method to study cavitation bubble dynamics. *Acustica* **26**, 170–171 (1972)
22. K.J. Ebeling, Hochfrequenzholografie mit dem Rubinlaser (High-speed holography with the ruby laser), *Optik* **48**, 383–397, 481–490 (1977)
23. W. Lauterborn, K.J. Ebeling, High-speed holography of laser-induced breakdown in liquids. *Appl. Phys. Lett.* **31**, 663–664 (1977)
24. W. Lauterborn, A. Judt, E. Schmitz, High-speed off-axis holographic cinematography with a copper-vapor-pumped dye laser. *Opt. Lett.* **18**, 4–6 (1993)
25. W. Hentschel, Hochfrequenzholografie mit dem Argon-Ionen Laser (High-speed holographic cinematography with the argon ion laser). *Optik* **68**, 283–310 (1984)
26. M. Novaro, Camera holographique ultra-rapide (Ultra high-speed holographic camera), *C. R. Acad. Sci. Paris, B.* **273**, 941–943 (1971)
27. W. Hentschel, W. Lauterborn, New speed record in long series holographic cinematography. *Appl. Opt.* **23**, 3263–3265 (1984)
28. W. Hentschel, W. Lauterborn, High speed holographic movie camera. *Opt. Eng.* **24**, 687–691 (1985)
29. W. Lauterborn, E. Cramer, Subharmonic route to chaos observed in acoustics. *Phys. Rev. Lett.* **47**, 1445–1448 (1981)
30. W. Lauterborn, A. Koch, Holographic observation of period-doubled and chaotic bubble oscillations in acoustic cavitation. *Phys. Rev. A.* **35**, 1974–1976 (1987)
31. W. Lauterborn, J. Holzfuss, Acoustic chaos. *Int. J. Bif. Chaos* **1**, 13–26 (1991)
32. W. Lauterborn, W. Hentschel, Cavitation bubble dynamics studied by high-speed photography and holography: Part two. *Ultrasonics* **24**, 59–65 (1986)
33. W. Lauterborn and W. Hentschel, Holografische Hochgeschwindigkeitskinematografie (Holographic high-speed cinematography), in *Praxis der Holografie (Practical holography)*, ed. by H. Marwitz et al. (Expert Verlag, Ehningen, 1989), pp. 354–370, 474–475
34. W. Lauterborn, T. Kurz, R. Mettin, C.D. Ohl, Experimental and theoretical bubble dynamics. *Adv. Chem. Phys.* **110**, 295–380 (1999)
35. W. Lauterborn and T. Kurz, Physics of bubble oscillations, *Rep. Prog. Phys.* 106501 (88 pp) (2010)
36. W. Lauterborn, Optische Kavitation (Optic cavitation). *Physikalische Blätter* **32**, 553–563 (1976)
37. W. Lauterborn, Cavitation and coherent optics, in *Cavitation and Inhomogeneities in Underwater Acoustics*, ed. by W. Lauterborn (Springer, Berlin, 1980), pp. 3–12
38. W. Hentschel, W. Lauterborn, Holographic generation of multi-bubble systems, in *Cavitation and Inhomogeneities in Underwater Acoustics*, ed. by W. Lauterborn (Springer, Berlin, 1980), pp. 47–53
39. K.Y. Lim, P.A. Quinto-Su, E. Klaseboer, B.C. Khoo, V. Venugopalan, C.-D. Ohl, Nonspherical laser-induced cavitation bubbles, *Phys. Rev. E.* **81**, 016308 (9 pp) (2010)
40. U. Schnars, W. Jüptner, Direct recording of holograms by a CCD target and numerical reconstruction. *Appl. Opt.* **33**, 179–181 (1994)
41. J. Sheng, E. Malkiel, J. Katz, Digital holographic microscope for measuring three-dimensional particle distributions and motions. *Appl. Opt.* **45**, 3893–3901 (2006)
42. G. Haussmann, W. Lauterborn, Determination of size and position of fast moving gas bubbles in liquids by digital 3-D image processing of hologram reconstructions. *Appl. Opt.* **19**, 3529–3535 (1980)

43. E. Malkiel, J.A. Abras, J. Katz, Automated scanning and measurement of particle distributions within a holographic reconstructed volume. *Meas. Sci. Technol.* **15**, 601–612 (2004)
44. U. Schnars, W. Jüptner, Digital recording and numerical reconstruction of holograms. *Meas. Sci. Technol.* **13**, R85–R101 (2002)
45. J. Katz, J. Sheng, Applications of holography in fluid mechanics and particle dynamics. *Annu. Rev. Fluid Mech.* **42**, 531–555 (2010)